Journal of Physics: Conference Series **318** (2011) 012001 doi:10.1088/1742-6596/318/1/012001

Turbulence in fluid layers

H. Xia[1], M. G. Shats[1] and G. Falkovich[2]

[1] Australian National University, Canberra ACT 0200, Australia
[2] Weizmann Institute of Science, Rehovot 76100, Israel

E-mail: gregory.falkovich@weizmann.ac.il

Abstract. Flows in natural fluid layers are often forced simultaneously at scales smaller and much larger than the depth. For example, Earth atmospheric flows are powered by gradients of solar heating: vertical gradients cause three-dimensional (3D) convection while horizontal gradients drive planetary scale flows. Nonlinear interactions spread energy over scales. The question is whether intermediate scales obtain their energy from a large-scale 2D flow or from a small-scale 3D turbulence. The paradox is that 2D flows do not transfer energy downscale while 3D turbulence does not support an upscale transfer. Here we demonstrate experimentally how a large-scale vortex and a small-scale turbulence conspire to provide for an upscale energy cascade in thick layers. We show that a strong planar vortex suppresses vertical motions thus facilitating an upscale energy cascade. In a bounded system, spectral condensation into a box-size vortex provides for a self-organized planar flow which secures an upscale energy transfer.

1. Introduction

Fluids naturally spread into layers under the action of gravity so that studying turbulence in layers is of both fundamental and practical importance. Turbulence in thin layers is quasi-two-dimensional. Considering an idealized 2D fluid, Kraichnan showed that if turbulence is forced at some intermediate wave number k_f, spectral energy flows upscales, towards smaller wave numbers, $k < k_f$, while enstrophy (integral of squared vorticity) flows downscales, toward higher wave numbers, $k > k_f$, where it is dissipated by viscosity (10). The kinetic energy spectra are given by $E(k) = C\epsilon^{2/3}k^{-5/3}$ in the inverse energy cascade range, $k < k_f$, and by $E(k) = C_q\eta^{2/3}k^{-3}$ for the small scales, in the forward enstrophy cascade range, $k > k_f$. Here ϵ and η are the dissipation rates of energy and enstrophy respectively, and C is the Kolmogorov constant. If no large-scale energy dissipation is present, energy cascades to larger and larger scales with no steady-state possible.

In the presence of a large-scale or uniform dissipation (e.g. bottom friction), energy delivered *via* the cascade will be dissipated. The maximum of the spectrum in this case will stabilize at some dissipation wave number given by $k_\alpha \approx (\alpha^3/\epsilon)^{1/2}$, where α is the linear dissipation rate. To achieve this steady state, the dissipation scale $2\pi/k_\alpha$ needs to be smaller than the system size L. This regime was studied experimentally (for example, (15; 16)) and numerically (12; 2). Energy spectra observed in the energy cascade range are close to the predicted $k^{-5/3}$ power law. Normalized third and fourth moments of the velocity suggest small non-Gaussianity and no signatures of the large-scale coherent structures (16; 2). The Kolmogorov constant is in the range of $C = 5.6 - 7$ (see (2) and references therein).

Similarly to 3D turbulence, Kolmogorov flux relation expresses the energy flux ϵ in the energy inertial range via the third-order velocity structure function S_3: $\epsilon \propto S_3/r$ (see e.g. (14; 26; 11)). The sign of S_3 is indicative of the direction of the energy cascade; positive S_3 corresponds to the inverse energy cascade (from small to large scales), while negative values indicate direct cascade.

If turbulence domain is bounded, the spectral energy may start accumulating at the box size. In the system with linear dissipation this occurs when the dissipation scale exceeds the box size, $2\pi/k_\alpha > L$. This energy pile-up at the scale close to the box size, referred to as spectral condensation, was predicted by Kraichnan and has been confirmed in numerical simulations (9; 20; 21; 7; 13; 5) and experimentally (22; 16; 17; 18; 23). In cases with zero damping (realized in numerics) the condensate grows, as shown by (20; 21; 5). When damping is present, the condensate is stabilized as a mean flow coherent over the system size and over many rotation periods, and the system as a whole achieves a statistically steady state.

One expects that in thick layers the flow is 3D and there is no inverse energy cascade. Indeed, as has been demonstrated in 3D numerical modeling, when the layer thickness exceeds half the forcing scale, the onset of vertical motions destroys turbulence quasi-two-dimensionality and stops the upscale energy transfer (19; 3). Here we report new laboratory studies of turbulence in layers which show that a large-scale horizontal vortex, either imposed externally or generated by spectral condensation in turbulence, suppresses vertical motions in thick layers. This leads to a robust inverse energy cascade even in thick layers. Brief presentation of the results has been published in (25).

2. Experimental setup

In our experiments turbulence is generated via the interaction of a large number of electromagnetically driven vortices. We use two different configurations: i) a single layer of electrolyte on a solid bottom, and ii) a layer of electrolyte on top of another layer of a non-conducting heavier liquid, which substantially decreases friction. In the latter case, a heavier non-conducting fluid (Fluorinert FC-77, specific gravity SG = 1.8) is placed at the bottom. A lighter conducting fluid, NaCl water solution (SG = 1.03), is placed on top. Both layers of fluids are placed in the spatially periodic vertical magnetic field produced by a square matrix of 30×30 permanent magnets (10 mm apart). This matrix is placed either underneath the fluid cell, or it is submerged in the Fluorinert. Two carbon electrodes are used to drive electric current (up to 3A) through the top layer. This current interacts with vertical magnetic field to generate 900 vortices ($\approx$ 9 mm in diameter) which produce turbulent quasi-2D flow. The electromagnetic forcing in this setup is detached from the bottom of the fluid cell, which helps to isolate the flow from the shear boundary layer. The dissipation due to the bottom drag can be controlled by changing the thickness of the fluid layers. The flow is limited by the walls of the fluid cell (0.3 $\times$ 0.3 m^2) and also by insertable square boundaries of the sizes $L = (0.09 - 0.24)$ m. Overall, the experimental setup is similar to those described in (16; 4; 18) but has a substantially larger number of forcing vortices, higher spatial resolution and larger scale separation ($L/l_f \approx 30$).

To visualize horizontal flows, imaging particles (polyamid, $50\mu m$, SG=1.03) are suspended in the top fluid layer and are illuminated using a 1 mm laser sheet parallel to the free surface. Laser light scattered by the particles is filmed from above using video camera (2 Mpixel) or a high resolution still camera (12.8 Mpixel) in the fast shooting mode. In the latter case two lasers, green and blue, are pulsed for 20 ms consecutively with a delay of (20-150) ms in between. In each still camera frame, two laser pulses produce a pair of images (green and blue) for each particle. The frame images are then split into pairs of images according to the colour. The velocity fields are obtained from these pairs of images using the cross-correlation particle image velocimetry technique. The velocity fields are measured every 0.33 s (at the camera shooting rate). For a better time resolution a video camera (25 fps) with a single laser is used. To visualize

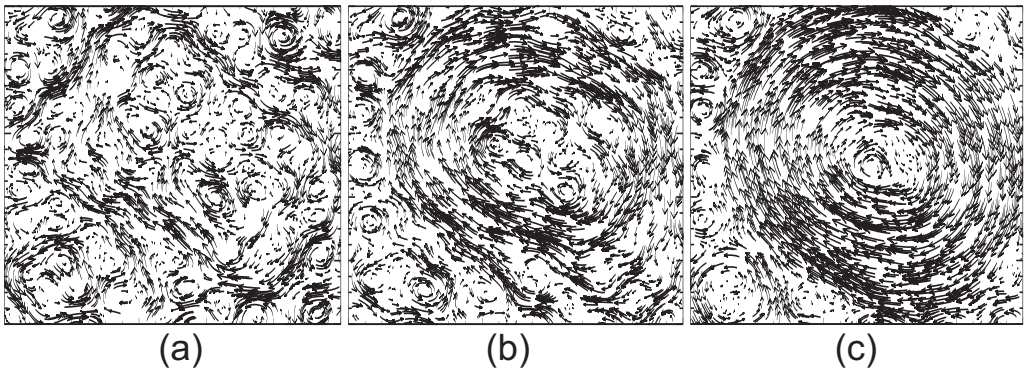

Figure 1. Time-averaged velocity fields of the condensate in the square box of $L = 0.1$ m at different thicknesses of the bottom fluid: (a) $\Delta h_b = 3$ mm, $\alpha = 0.25$ s^{-1}, (b) $\Delta h_b = 4$ mm, $\alpha = 0.15$ s^{-1} and (c) $\Delta h_b = 5$ mm, $\alpha = 0.05$ s^{-1}.

vertical flows, a vertical laser slab is used and the particle motion is filmed from the side. To quantify the velocity fluctuations in 3D, a defocusing PIV technique has been developed, which allows all 3 velocity components to be measured (24).

The linear damping rate α is controlled by changing the thickness of the two fluid layers. Damping rates in the range of $\alpha = 0.05 - 0.5$ s^{-1} are achieved. A damping rate is estimated from the decay of the energy density after switching off the forcing at $t = t_0$: $E_t = E_{t_0} e^{-\alpha(t-t_0)}$.

To ensure that there is no significant ripple on the free surface of the fluid, we use a laser-reflection technique to measure spectra and the amplitude of the surface ripple. We find that at modest forcing used in our experiments the potential energy contribution (due to the ripple) is several orders of magnitude smaller than the kinetic energy of the flow related to horizontal velocities.

It should be noted that recent reports on intrinsic three-dimensionality of the electromagnetically driven shallow flows (e.g., (1)) have not been confirmed in our experiments: three-dimensional flow features were observed only for a single-layer electrolyte of thickness comparable to the forcing scale. Stratified fluid configurations with the layer thickness of less than 5 mm each do not show any 3D effects.

3. Thin layer

Spectral condensation has been reported in thin layer experiments (22; 16; 17) as generation of a monopole vortex. We generate the condensate at three different linear damping rates within the square boundary of size $L = 0.1$ m. Time-averaged (over 150 s) velocity fields of the flow after the emergence of the spectral condensate are shown in Fig. 1 for three different thicknesses of the bottom layer, $\Delta h_b = 3, 4$ and 5 mm. The time evolution of the energy density E_0 after forcing is switched off is shown in Fig. 2. These measurements are used to estimate the damping rates for different Δh_b. Damping plays a very important role for the symmetry of the condensate vortex. The vortex turn-over time is estimated using the maximum azimuthal velocity of the flow and the diameter of the vortex corresponding to this maximum velocity.

The condensate vortex becomes more symmetric as the vortex turnover time τ_{to} approaches the damping time $\tau_d \approx 1/\alpha$, as in Fig. 1 (c). When τ_d is approximately one-third of the turn-over time, the vortex is less symmetric, Fig. 1 (b). For the least symmetric case of Fig. 1 (a), the damping time is only 4 s comparing to an eddy turn-over time of about 40 s.

Fig. 3 shows moments of velocity for the case of the condensate of an intermediate strength generated within a smaller boundary, $L = 0.15$ m, and at lower damping, $\alpha \approx 0.15$ s^{-1}. In this

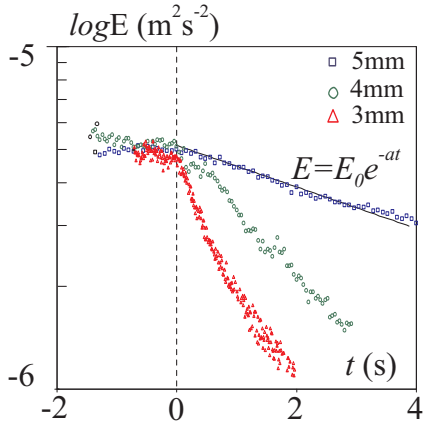

Figure 2. Vortex decay.

case the energy spectrum shows three different power laws: $E_k \propto k^{-(3-4)}$ for small and large scales, and $k^{-5/3}$ in the intermediate range of wave numbers, $k_t < k < k_f$, Fig. 3 (a). The third-order structure function, however, changes dramatically in this case: S_3 becomes negative in the range of scales $2\pi/k_f < r < 2\pi/k_t$, while at larger scales, $r > 2\pi/k_t$, S_3 is positive and the $S_3(r)$ dependence is not linear as seen in Fig. 3 (b). Flatness and skewness are shown in Fig. 3 (c). These normalized moments show much larger variability with r compared with the weak condensate. Since turbulence in these experiments is forced at small scales, negative S_3 cannot be indicative of the direct (downscales) cascade. The change in S_3 compared with the weak condensate case must be attributed to the formation of the large-scale mean shear flow resulting from spectral condensation.

Indeed, in the presence of the spectral condensate, the flow velocity and its increments contain both mean and fluctuating velocity components, $\delta V = \delta\bar{V} + \delta\tilde{V}$. The second-order structure function contains not only second moment of velocity fluctuations $\delta\tilde{V}^2$, but also two other terms, $\left\langle \delta V^2 \right\rangle = \left\langle \delta\bar{V}^2 + 2\delta\bar{V}\delta\tilde{V} + \delta\tilde{V}^2 \right\rangle$. The second term averages out. The third-order moment is affected more: $\left\langle \delta V^3 \right\rangle = \left\langle \delta\bar{V}^3 - 3\delta\bar{V}^2\delta\tilde{V} + 3\delta\bar{V}\delta\tilde{V}^2 - \delta\tilde{V}^3 \right\rangle$. Again, the term with $\delta\tilde{V}$ averages to zero, while the terms $< \delta\bar{V}^3 >$ and $< 3\delta\bar{V}\delta\tilde{V}^2 >$ modify the third velocity moment in the presence of the mean shear flow.

To recover statistical moments and spectra of underlying turbulence from the measured total velocity fields, we subtract mean time average velocity $\bar{V}(x,y) = (1/n_t)\sum_{n=1}^{n_t} V(x,y,t_n)$ from n_t instantaneous velocity fields and repeat the above analysis. Figure 4 shows the results. The energy spectrum now shows $E(k) \propto k^{-5/3}$ power law over (almost) the entire spectral range, Fig. 4 (a). The scatter in the spectrum after mean subtraction is reduced compared with Fig. 3 (a). This actually supports the suggestion that even the second moment is "polluted" by the mean $< \delta\bar{V}^2 >$ component of the flow.

The third-order structure function is positive in the energy cascade range of scales, Fig. 4 (b), i.e. corresponds to an inverse cascade, as expected. At scales corresponding to $2\pi/k_f < r < 2\pi/k_t$, S_3 is a linear function of r. The spectral energy flux in this range is estimated as $\epsilon = S_3/r$. Let us stress the necessity to subtract the coherent part of the flow to recover not only value but even the sign of the flux. It may bear relation to the meso-scale atmospheric turbulence where signs of a direct cascade may be due to a contamination by large-scale flows.

Figure 4 (c) shows flatness and skewness in after mean subtraction. In the presence of the stronger condensate, skewness at scales larger than the forcing scale is small but positive, $Sk = (0.02 - 0.05)$. Flatness is higher when the condensate is stronger.

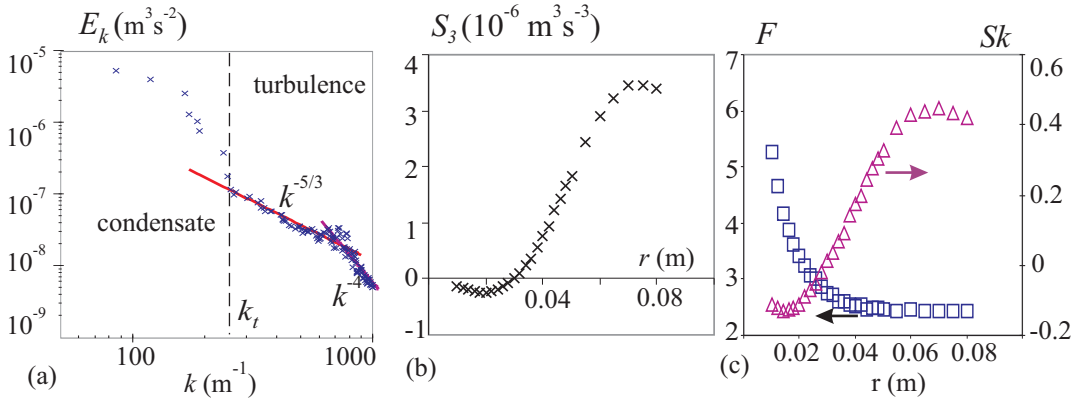

Figure 3. Intermediate-strength spectral condensate in the $L = 0.15$ m boundary box, linear damping $\alpha \approx 0.15$ s^{-1}. (a) Energy spectrum, (b) the third-order structure function, and (c) flatness (squares) and skewness (triangles) as functions of the separation distance r.

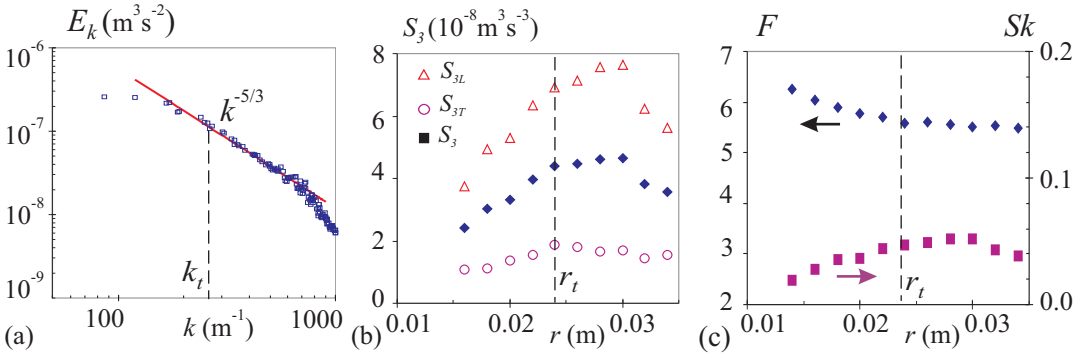

Figure 4. (a) Energy spectrum, (b) longitudinal (triangles), transverse (circles) and full (squares) third-order structure functions and (c) normalized velocity moments F and Sk computed after the subtraction of the mean flow from $N = 350$ instantaneous velocity fields in the intermediate condensate case. Vertical dashed lines indicate the wave number and the scale corresponding to the knee in the spectrum of Fig. 3 (a).

4. Thick layer

We present the results starting with a thick two-layer configuration when the top layer thickness h_t exceeds half the forcing scale l_f. The forcing scale in this experiment is $l_f = 9$ mm while the thicknesses of the bottom and top layers are $h_b = 4$ mm and $h_t = 7$ mm respectively. The size of the boundary box is $L = 120$ mm. Turbulence is forced electromagnetically by the array of magnetic dipoles, $l_f = 9$ mm, in the top layer of electrolyte ($h_t = 7$ mm) resting on the 4 mm layer of non-conducting heavier liquid. Particle streaks are filmed in the horizontal x-y plane with the exposure time of 2 s (a,c) and in the vertical z-y plane with the exposure time of 1 s (b,d) during the development of the large scale vortex.

Visualization in both horizontal (x-y) and vertical (z-y) planes shows that the flow is substantially 3D at the early stage of the evolution, as seen in Figs. 5(a,b,c,d), in agreement with numerics. If however one waits long enough, one sees the appearance of a large planar vortex whose diameter is limited by the box size (that effect was avoided in numerical simulations by limiting the analysis time). Apparently, a residual inverse energy flux, existing even in the presence of 3D motions, leads to the spectral condensation and to the generation of the large

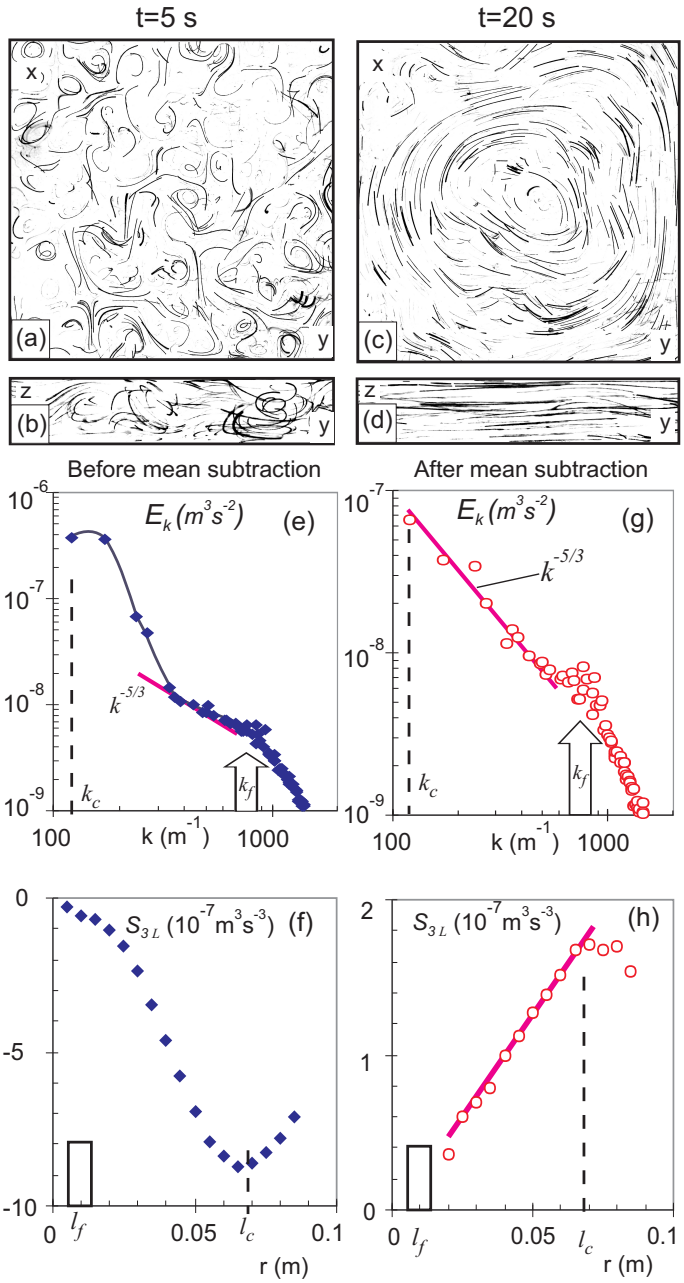

Figure 5. Structure of turbulence in the double layer configuration. Images (a,b) correspond to the time interval centered around $t = 5$ s after the flow forcing is switched on; (c,d) correspond to $t = 20$ s. The size of the horizontal plane box is 120 mm, the thickness of the top layer in (b,d) is 7 mm. The spectrum of the steady flow (e) and the third-order structure function S_{3L} (f) are dominated by the contribution from the large coherent vortex (c), which develops as a result of turbulence spectral condensation. Subtraction of the mean velocity field reveals the spectrum (g) and S3L (h), which are similar to those in quasi-2D turbulence.

coherent vortex which dominates the flow in a steady state, Fig. 5(ca). In the vertical cross-section the flow is now close to planar, Fig. 5(db). The vortex gives a strong spectral peak at $k \simeq k_c$, as seen in Fig. 5(e), where k_f is the forcing wave number corresponding to the forcing scale. The subtraction of the temporal mean reveals the spectrum of the underlying turbulence, see Fig. 5(g), which shows a reasonably good agreement with the Kraichnan $k^{-5/3}$ inverse energy cascade. Similarly, before the mean subtraction, reveals positive linear S_3, Fig. 5(h). Before the mean subtraction S_3 is negative and is not a linear function of r, Fig. 5 (f). The subtraction of the mean vortex flow reveals positive S_3, which is a linear function of r in agreement with (1), Fig. 5(h). The slope of that linear dependence gives the value of the upscale energy flux, $\epsilon \simeq 1.8 \cdot 10^{-6}\, m^2/s^3$. This value was independently verified by the energy balance analysis, as described (23): ϵ is compared with the rate of the large-scale flow decay similar to the one shown in Fig. 2. For the present experiment this agreement is within ten percent.

The results of Fig. 5 suggest that, contrary to expectations, turbulence in a thick layer ($h_t/l_f = 0.78$) supports the inverse energy cascade, as evidenced by the S_3 result, and also by the generation of the strong spectral condensate fed by the cascade. Similar results were obtained in even thicker layers, up to $h_t/l_f = 1.38$. Strong spectral condensates whose energy constitutes above ninety percent of the total flow energy of the flow are observed in those cases. After the development of the condensate, particle streaks are almost planar as seen in Fig. 5(db). Thus, there must be a mechanism through which the vortex secures its energy supply by suppressing vertical motions and enforcing the flow planarity. To investigate the effect of a large flow on 3D turbulent motion, we perform experiments in a single layer of electrolyte, $h = 10$ mm, with much larger boundary, $L = 300$ mm, to avoid spectral condensation. In this case the large-scale vortex is imposed externally. The timeline of the experiment is shown schematically in Fig.2(a). First, turbulence is excited. Then a large vortex (150 mm diameter) is imposed on it by placing a magnetic dipole 2 mm above the free surface. After the large magnet is removed, the vortex decays, while turbulence continues to be forced. Since the large magnet blocks the view, the measurements are performed during the turbulence stage and during the decay of the vortex. Figure 6(b) shows the profiles of the vertical velocity fluctuations, measured using defocusing PIV. Before the vortex is imposed, vertical fluctuations are high, $V_{z,rms} \simeq 1.6$ mm/s. When the vortex is present, they are reduced by a factor of about 4, down to $V_{z,rms} \simeq 0.4$ mm/s. This is also confirmed by the direct visualization of the flow in the vertical z-y plane. Particle streaks are shown in Figs. 6(c-e). Strong vertical eddies are seen in the turbulence stage, before the vortex is imposed, Fig. 6(c). Shortly after the large magnet is removed, at $t - t_0 = 1$ s, the streaks show no vertical excursions. As the large vortex decays, the 3D eddies start to reappear near the bottom, Fig. 6(e). We also study the statistics of the horizontal velocities. The kinetic energy spectra and the third-order moments are shown in Figs. 6(f-h). For turbulence without the vortex, the spectrum is substantially flatter than $k^{-5/3}$, Fig. 6(f). After the large vortex is imposed, the spectrum shows a strong peak at low wave numbers. The mean subtraction however recovers $k^{-5/3}$ 2D spectrum, as shown in Fig. 6(g). The third-order moment undergoes even more dramatic change after the imposition of the large vortex: S_{3L} computed after the mean subtraction is much larger than during the turbulence stage, and it is a positive linear function of r, Fig. 6(h), just as in the case of the double-layer experiment. Thus the imposed flow enforces planarity and strongly enhances the inverse energy flux.

The strong suppression of vertical eddies in the presence of an imposed flow must be due to the vertical shear S which destroys vertical eddies whose inverse turnover time is less than S. We estimate the value of this shear from the z-profiles of the horizontal velocity measured using defocusing PIV. In a single-layer experiment, the averaged shear of the horizontal velocity due to the presence of strong imposed vortex is $S \simeq 1.6$ 1/s. Such a shear is sufficient to suppress vertical eddies whose inverse turnover time is $V_{z,rms}/h \simeq 0.16$ 1/s. In the spectrally condensed turbulence, an inverse energy cascade is sustained in layers which are substantially thicker than

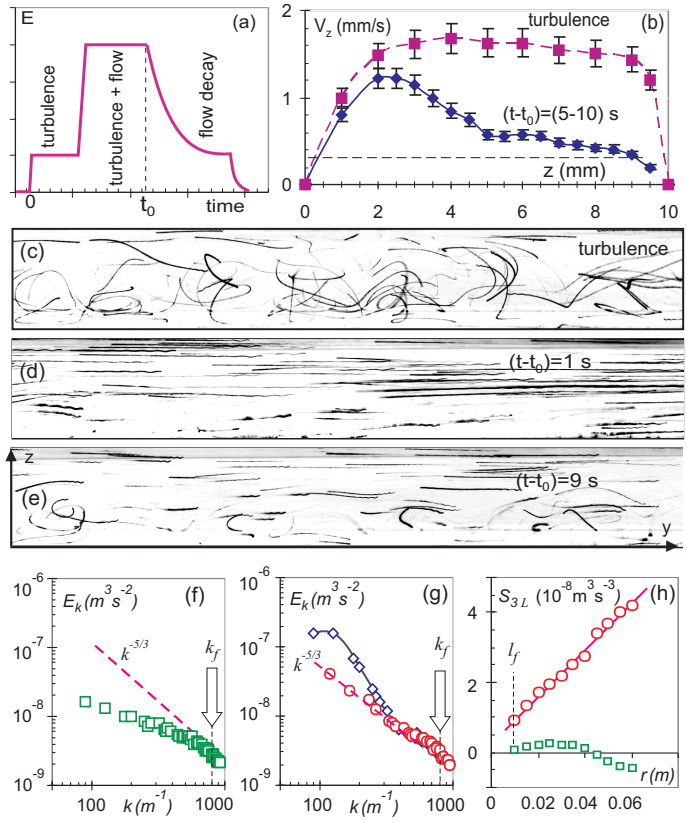

Figure 6. Effects of externally imposed large-scale flow on turbulence in a single fluid layer. (a) The time line of the experiment: turbulence forcing is switched on, then, 100 seconds later, a large scale vortex (150 mm diameter) is imposed on top of turbulence. The vortex forcing is then removed at t_0. The large vortex decays, while turbulence is still forced. Measurements using defocusing PIV technique show that vertical velocity fluctuations are substantially reduced by the large-scale vortex (b). Error bars correspond to 10% instrumental accuracy of the technique. Streaks of seeding particles filmed in the vertical (z-y) cross-section (c) show strong 3D motion before the large-scale vortex is imposed (exposure time is 2 s). Particle streaks filmed during the decay of the large-scale vortex (exposure time is 1 s) show that vertical motions are suppressed (d). As the vortex decays further, 3D eddies re-emerge from the bottom of the cell (e). The spectrum of horizontal velocities is flat in turbulence (f). During the decay of the large vortex the spectrum is dominated by the low-k spectral feature, open diamonds in (g). The subtraction of the mean flow recovers the $k^{-5/3}$ cascade range, open circles (g). The third-order structure function S_{3L} computed after the mean subtraction is a positive linear function of the separation distance, open circles (h). S_{3L} in the turbulence stage is much smaller, open squares (h).

it is possible in unbounded turbulence. A possible reason for this is also the shear suppression of the 3D vortices. Here the vertical shear is lower, $S \simeq 0.5$ 1/s, yet it exceeds substantially the inverse turnover time for the force-scale vortices in the double-layer experiment, $V_{z,rms}/h \simeq 0.06$ 1/s. One may think that the dramatic change in the flow field in the presence of the large vortex is due to the global fluid rotation. However, the Rossby numbers in the reported experiments are larger (especially in the double layer experiment, $Ro > 3$) than those at which quasi-2D flow properties were observed in rotating tanks ($Ro < 0.4$).

Figure 7 shows vertical profiles of vertical V_z and horizontal V_x, V_y velocities for the case of a double layer. In all cases, top 3 mm of the bottom layer is reasonably planar.

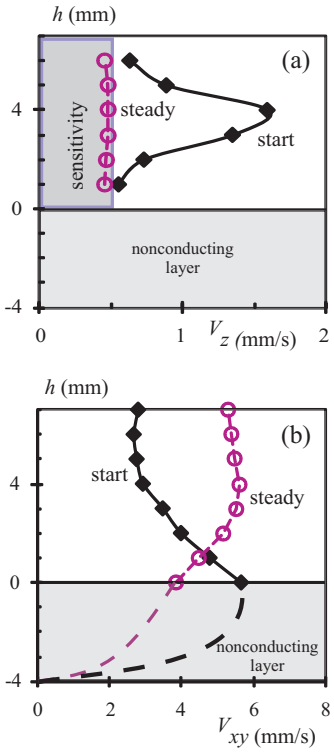

Figure 7. Vertical profiles of vertical V_z and horizontal V_x, V_y velocities for the case of a double layer. Two profiles in each panel correspond to the early stage of the flow evolution (Fig. 6a-b) and to the steady state. The velocities shown are the rms velocities (without mean subtraction). In the beginning there is a contribution of forcing (Fig.b) near the interface between two layers (maximum forcing). Later, as the condensate develops, mean flow shows up, which also sweeps forcing vortices, reducing rms(V) near the interface. Dashed lines show expected (not measured) velocities.

The suppression of vertical motions by the shear flow and the onset of the inverse cascade observed in this experiment may be relevant for many natural and engineering applications. In the solar tachocline, a thin layer between the radiative interior and the outer convective zone, turbulence is expected to be 2D, despite being excited by radial convection. Present results suggest that only one velocity component can be strongly suppressed, making turbulence 2D. Another interesting example is the wave number spectrum of winds in the Earth atmosphere measured near the tropopause2, which shows in the mesoscale range (10-500 km) and a strong peak at the planetary scale of 104 km (8). Numerous hypotheses have been suggested to explain the mesoscale spectrum with most arguments centered on the direct versus the inverse energy cascade. The shape of the spectrum alone cannot resolve this issue since both the 3D Kolmogorov direct cascade and the 2D Kraichnan inverse cascade predict . Direct processing of atmospheric data gave for some range of r in mesoscales, thus favoring the direct cascade hypothesis (11; 6). However, the subtraction of the mean flows, necessary for the correct flux evaluation, has not been done for the wind data. This leaves the question about the source of the mesoscale energy unresolved. Estimates of the vertical shear due to the planetary scale flow represented by the spectral peak at 104 km show that the shear suppression criterion can be satisfied for the small-scale eddies with sizes less than 10 km. Thus, it is possible that the suppression of 3D vertical eddies induces an inverse energy cascade through the mesoscales in the Earth atmosphere. Moreover, our results may be relevant not only for thin layers but also for boundary layer flows with extra turbulence (generated by surface roughness, convection or other reasons), and may shed light on the nature of velocity correlations at the horizontal distances far exceeding the distance from the ground, which is important for wind farms and many other problems.

4.1. Acknowledgments

This work was supported by the Australian Research Council's Discovery Projects funding scheme (DP0881544) and by the grants of the Minerva Foundation and the Israeli Science

Foundation.

References

[1] Akkermans, R.A.D., Kamp, L.P.J., Clercx, H.J.H. & van Heijst, G.J.F. 2008,Intrinsic three-dimensionality in electromagnetically driven shallow flows,*Europhys. Lett.* **83** 24001.

[2] Boffetta, G., Celani, A. & Vergassola, M. 2000 Inverse energy cascade in two-dimensional turbulence: Deviation from Gaussian behavior. *Phys. Rev. E* **61**, R29.

[3] Celani, A., Musacchio, S. and Vincenzi, D. 2010 Turbulence in more than two and less than three dimensions. *Phys. Rev. Lett.* **104**, 184506.

[4] Chen, S., Ecke, R.E., Eyink, G.L., Rivera, M., Wan, M. & Xiao, Z. 2006 Physical mechanism of the two-dimensional inverse energy cascade. *Phys. Rev. Lett.* **96**, 084502.

[5] Chertkov, M., Connaughton, C., Kolokolov, I. & Lebedev, V. 2007 Dynamics of energy condensation in two-dimensional turbulence. *Phys. Rev. Lett.* **99**, 084501.

[6] Cho, J.Y.N. & Lindborg, E. 2001 Horizontal velocity structure functions in the upper troposphere and lower stratosphere 1; Observations. *J. Geophys. Res.* **106**, 10223.

[7] Dubos, T., Babiano, A., Paret, J. & Tabeling, P. 2001 Intermittency and coherent structures in the two-dimensional inverse energy cascade: comparing numerical and laboratory experiments. *Phys. Rev. E* **64**, 036302.

[8] Gage, K.S. & Nastrom, G.D. 1986 Theoretical interpretation of atmospheric wavenumber spectra of wind and temperature observed by commerical aircraft during GASP. *J. Atm. Sci.* **43**, 729.

[9] Hossain, M., Matthaeus, W.H. & Montgomery, D. 1983 Long-time states of inverse cascades in the presence of a maximum length scale. *J. Plasma Physics* **30**, 479.

[10] Kraichnan, R. 1967 Inertial ranges in two-dimensional turbulence. *Phys. Fluids* **10**, 1417.

[11] Lindborg, E. 1999 Can the atmospheric kinetic energy spectrum be explained by two-dimensional turbulence? *J. Fluid Mech.*, **388**, 259.

[12] Maltrud, M.E. & Vallis, G. K. 1991 Energy spectra and coherent structures in forced two-dimensional and beta-plane turbulence. *J. Fluid Mech.*, **228**, 321.

[13] Molenaar, D., Clercx, H.J.H. & van Heijst, G.J.F. 2004 Angular momentum of forved 2D turbulence in a square no-slip domain. *Physica D* **196**, 329.

[14] Monin, A.S.& Yaglom A.M., *Statistical Fluid Mechanics* (MIT, Cambridge Mass.,1975), Vol.2.

[15] Paret, J. & Tabeling, P. 1997 Experimental observation of the two-dimensional inverse energy cascade. *Phys. Rev. Lett.* **79**, 4162.

[16] Paret, J. & Tabeling, P. 1998 Intermittency in the two-dimensional inverse cascade of energy: Experimental observations. *Phys. Fluids* **10**, 3126.

[17] Shats, M.G., Xia, H. & Punzmann, H. 2005 Spectral condensation of turbulence in plasmas and fluids and its role in low-to-high phase transitions in toroidal plasma. *Phys. Rev. E* **71**, 046409.

[18] Shats, M.G., Xia, H.,Punzmann, H. & Falkovich, G. 2007 Suppression of turbulence by self-generated and imposed mean flows. *Phys. Rev. Lett.* **99**, 164502.

[19] Smith, L.M., Chasnov, J.R. and Fabian, W. 1996 Crossover from two- to three-dimensional turbulence. *Phys. Rev. Lett.* **77**, 2467-2470.

[20] Smith, L. & Yakhot, V. 1993 Bose condensation and small-scale structure generation in a random force driven 2D turbulence. *Phys. Rev. Lett.* **71**, 352.

[21] Smith, L. & Yakhot, V. 1994 Finite-size effects in forced two-dimensional turbulence. *J. Fluid Mech.* **274**, 115.

[22] Sommeria, J. 1986 Experimental study of the two-dimensional inverse energy cascade in a square box. *J. Fluid Mech.* **170**, 139.

[23] Xia, H., Punzmann, H., Falkovich, G. & Shats, M.G. 2008 Turbulence-condensate interaction in two dimensions. *Phys. Rev. Lett.* **101**,194504.

[24] Willert C.E. and Gharib M. 1992 Three-dimensional particle imaging with a single camera. Experiments in Fluids, 12, 353-358.

[25] Xia H , Byrne D , Falkovich G , Shats M 2011 Upscale energy transfer in thick turbulent fluid layers. *Nature Physics* **7**, 321-324

[26] Yakhot, V. 1999 Two-dimensional turbulence in the inverse cascade range. *Phys. Rev. E* **60**, 5544.